Effect of crystal defects in iron on carbon diffusivity: Analytical model married to atomistics

Sebastián Echeverri Restrepo [*]

SKF Research & Technology Development (RTD), SKF B.V., Meidoornkade 14, 3992 AE Houten, The Netherlands
and Department of Physics, King's College London, Strand, London WC2R 2LS, United Kingdom

Predrag Andric

SKF Research & Technology Development (RTD), SKF B.V., Meidoornkade 14, 3992 AE Houten, The Netherlands

Anthony T. Paxton

Department of Materials, Imperial College London, South Kensington Campus, London SW7 2AZ, United Kingdom

We devise a scheme for simulating diffusion of interstitial solutes in metals when the diffusivity is modified by the presence of defects. The method is quite general and may be used to model the effects of more than one defect in combination. In addition, it is amenable to being described by a simple analytic model fitted to a small number of parameters that can be determined by computer experiments. Using classical interatomic potentials and molecular dynamics, we calculate the diffusivity of carbon in iron and study the effects of a substitutional alloying element and an edge dislocation. Some of our results are validated against published experimental findings and previous simulations, and we are able to apply our theoretical model to rationalize our results and to show how, once the model is fitted to the computer experiments, it may be used in a predictive manner.

Steel is the most ubiquitous structural material and, according to the World Steel Association, demand is predicted to increase to six billion sterling by 2030. It is a material enjoying continuous development: more than three-quarters of the current grades have been designed in the last 20 years [1]. The SpaceX Starship will be made from steel [2]. The heart of the issue is the behavior of carbon (C) in iron (Fe), since it is this alloying element that distinguishes Fe from steel. The effect of this interstitial element is key to the understanding of a myriad of phenomena. Building up on recent developments on the study of the diffusion C in Fe [3–9], we devise a scheme for simulating diffusion of interstitial solutes in metals, such as C in Fe, when the diffusivity is modified by the presence of defects.

The effect that substitutional alloying elements in Fe have in the diffusion of C, has been studied in the literature using density functional theory and kinetic Monte Carlo simulations [10,11]. It was found that the addition of solutes to Fe can greatly affect the distribution and chemical potential of C, and that different alloying elements can have more or less pronounced effects on the diffusivity of C.

The interaction of diffusing C with dislocations has also received some attention in the literature. In Ref. [12], the concept of conjugate direction of migration was proposed. It was found that C does not necessarily diffuse along the dislocation line, but along a conjugate direction that is a function of the character of the dislocation. A key observation was that C and the dislocation move as a codiffusing complex and not as separate entities. This effect arises from the role that C plays in stabilizing a kink in the dislocation line: a segment of dislocation is attracted to a C atom to generate a thermally activated kink. In this way, the dislocation advances crabwise, with kinks appearing simultaneously with the migration of the C atom along the dislocation line. We observe exactly this effect in the simulations reported here, as will be discussed later in this Letter.

In the current Letter, we build up on previous work [13] to propose a simplified Arrhenius-based model for the diffusion of an interstitial atom (C) within a base uniform lattice (Fe) in the presence of defects (substitutional alloying elements, dislocations) in the dilute limit. We derive an analytical expression to calculate the diffusivity of C as a function of a defect density and temperature. In principle, the defects can take any shape, but here we will focus on substitutional atoms (*point defects*) and edge dislocations (*line defects*).

Diffusion of an interstitial atom in a cubic crystal is described by Einstein's equation for diffusivity,

$$D = \frac{1}{6}zd^2\nu, \tag{1}$$

in which $z = 4$ is the number of neighboring octahedral sites in the Body Centred Cubic (BCC) lattice, $d = a_0^{\text{Fe}}/2$ is the distance between them, and ν is the probability per unit time that the C atom makes a jump into one of the former. For systems containing defects, the background energy landscape is no longer homogeneous; the diffusional behavior of an interstitial atom cannot be properly described using a single energy barrier.
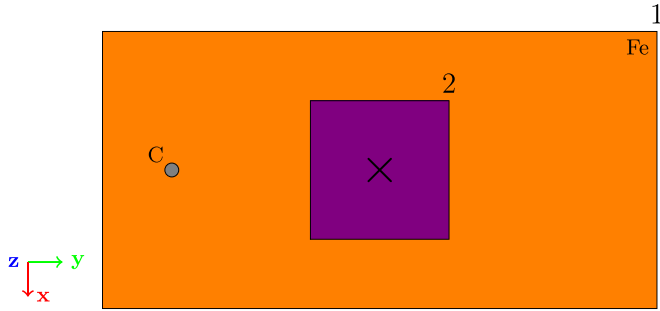
————————
[*] sebastian.echeverri.restrepo@skf.com

FIG. 1. Schematic view of the simulation systems containing a C atom and a crystallographic defect ($\times$) embedded in a BCC Fe lattice. Region 1 (in orange) is defect-free and has the same properties of bulk Fe. Region 2 (in purple) surrounds the defect and acts as a medium with different average diffusional properties.

Consider a periodic model system containing a single defect and a C interstitial atom in an otherwise homogeneous BCC-Fe lattice, see Fig. 1. We divide the system into two regions: region 1 is located away from the defect while region 2 contains the defect. The defect density can be effectively controlled by changing the size of region 1 while keeping the size of region 2 fixed. The probability, P_i, for the C atom to be found in region i (for $i = 1, 2$) is given by

$$P_i = \frac{g_i e^{-E_i/k_B T}}{\sum_{j=1}^m g_j e^{-E_j/k_B T}}, \tag{2}$$

where g_i is the number of octahedral sites in region i, E_i is an equivalent binding energy for region i, and $m = 2$ is the number of regions. Note that, in principle, m could take larger values in systems simultaneously containing various noninteracting defect types.

The probability density, ν_i, that the C atom makes a jump between two sites while being in region i is given by the Boltzmann formula,

$$\nu_i = \nu_i^0 \, e^{-\varepsilon_i/k_B T}, \tag{3}$$

where ε_i is an equivalent energy barrier between octahedral sites for region i, and ν_i^0 is a normalizing prefactor, or attempt frequency.

We can combine the two previous equations and assert that the diffusivity of the interstitial C atom in the system is given by

$$D = D_0^{\text{eff}} \sum_{i=1}^m P_i \nu_i, \tag{4}$$

where D_0^{eff} is an effective prefactor. Once the values of E_i and ϵ_i are identified, Eq. (4) is valid across range of temperatures and defect densities/concentrations.

We now evaluate the robustness of Eq. (4) against Molecular Dynamics (MD) simulations for the following three cases: (i) diffusion in bulk Fe, (ii) diffusion in the presence of substitutional solutes, and (iii) diffusion in the presence of edge dislocations. The values of E_i and ϵ_i are estimated by fitting Eq. (4) to MD results obtained at temperatures of 1023.15 K, 923.15 K, 823.15 K, and 723.15 K at, if any, a single value of defect density/concentration. The temperatures are chosen to

enable sufficiently fast diffusion while keeping the underlying BCC lattice stable.

In the case of a homogeneous system with only one region (one value for the energy barriers), like C in Fe, Eq. (4) reduces to the Arrhenius equation, since $P_i = P_1 = 1$,

$$D = D_0 e^{-\varepsilon/k_B T}, \tag{5}$$

in which $D_0 = zd^2\nu_0/6$, and ε is the activation enthalpy. For the calculations performed in this paper, we make the following approximations: $\nu_i^0 = \nu_0$ and $D_0^{\text{eff}} = D_0/\nu_0$.

The results of the diffusivity simulations of C in bulk Fe are presented in Fig. 2(a), marked with the labels bulk Embedded Atom Method (EAM) and bulk Modified Embedded Atom Method (MEAM), together with a fit to Eq. (5). A detailed description of the simulation procedure and the methodology to calculate the diffusivity from MD is presented in the Supplemental Material [14] [3,5,8,13,15–35]. As expected, there is an inverse relation between the two quantities, a clear signature of a single rate-limited thermally activated process. The calculation is performed for two interatomic potentials, one (developed in Refs. [25,26]) based on the EAM [22–24] and another (developed in Ref. [30]) based on the MEAM [27–29] formalisms. We obtain energy barriers for the migration of C between adjacent octahedral sites of $\varepsilon^{\text{EAM}} = 0.79$ eV and $\varepsilon^{\text{MEAM}} = 0.71$ eV and values for the prefactor of $D_0^{\text{EAM}} = 6.99 \times 10^{-7}$ m^2 s^{-1} and $D_0^{\text{MEAM}} = 1.97 \times 10^{-7}$ m^2 s^{-1}. More details about the interatomic potentials used in this paper can be found in the Supplemental Material [14].

The diffusion of C in the presence of substitutional solutes is simulated using the Fe-Ti-C MEAM potential [30]. We use Eq. (4) and the method described above to predict the diffusivity of C in a system of BCC Fe containing different concentrations of Ti atoms. We want to capture the effect that a substitutional atom has on the diffusivity of C in BCC Fe.

We start by expanding Eq. (4) for a system that contains two regions (see Fig. 1): Region 2 will be defined as a cube of size $2.5 \times 2.5 \times 2.5$ Fe lattice parameters (a_0^{Fe}) centered in the Ti atom. Region 1 encompasses the rest of the atoms in the system, whose behavior can be approximated by that of bulk BCC Fe. The expanded Eq. (4) is given by

$$
\begin{aligned}
D = D_0^{\text{eff}} \Bigg[&\frac{g_1 e^{-E_1/(k_B T)}}{g_1 e^{-E_1/(k_B T)} + g_2 e^{-E_2/(k_B T)}} \nu_{1,0} e^{-\varepsilon_1/(k_B T)} \\
&+ \frac{g_2 e^{-E_2/(k_B T)}}{g_1 e^{-E_1/(k_B T)} + g_2 e^{-E_2/(k_B T)}} \nu_{2,0} e^{-\varepsilon_2/(k_B T)} \Bigg].
\end{aligned} \tag{6}
$$

In the above equation, there are four unknown variables that need to be extracted from MD simulations, namely, E_1, ε_1, E_2, and ε_2. Since the atoms in region 1 are far from the Ti atom, we can assign to ε_1 the value obtained previously for C diffusion in bulk BCC Fe. We thus have that $\varepsilon_1 = \varepsilon^{\text{MEAM}} = 0.71$ eV. We define $E_1 = 0$ to be the reference point for measuring energies.

We proceed to the calculation of E_2 and ε_2 using MD simulations. A periodic system of BCC Fe atoms of size $6 \times 6 \times 6\,a_0^{\text{Fe}}$ is generated, one of the Fe atoms is replaced by a Ti atom (for a Ti concentration of 0.23 at. %), and a single interstitial C atom is introduced. We define the size of region 2 to be $2.5 \times 2.5 \times 2.5\,a_0^{\text{Fe}}$. The resulting diffusivities from
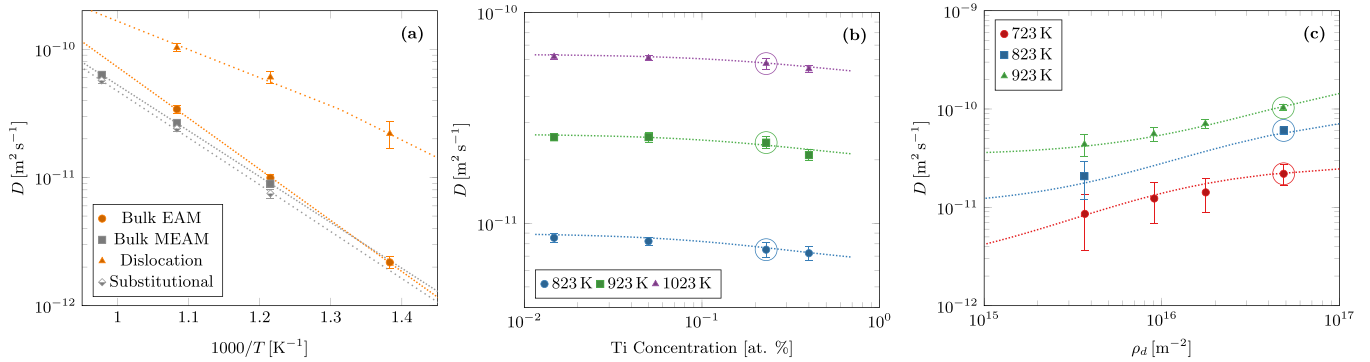
FIG. 2. Arrhenius plot of the effective diffusivities (D) for systems containing (a) a single C atom or a single C atom and a crystallographic defect inside a BCC lattice of Fe atoms and a fixed defect density. (b) Results for different Ti concentrations. (c) Results as a function of the density of dislocations. The symbols represent the results of MD simulations, while the lines are fits to Eq. (6). Large circles surround the results that were used for fitting the model (b), (c)

the MD simulations are presented in Fig. 2(a), marked with the label "substitutional," together with a fit to Eq. (4). From the fit, we extract the following values: $E_2 = -0.12\,\text{eV}$ and $\varepsilon_2 = 0.73\,\text{eV}$. The negative value of the binding energy E_2 indicates that the diffusing C atom will have the tendency to remain close to the substitutional Ti. The value of the migration energy barrier $\varepsilon_2 = 0.73\,\text{eV}$, which is slightly higher than that of the bulk ($\varepsilon_1 = 0.71\,\text{eV}$), indicates that the presence of Ti will cause a reduction of the diffusivity of C.

In Fig. 2(b), we test the predictive capabilities of Eq. (4) with respect to MD simulations. We present results for simulations with varying box sizes (and hence, concentrations of Ti atoms) and temperatures. We consider four concentrations, namely, 0.015, 0.05, 0.23, and 0.4 at. %. The data points used for fitting are shown surrounded by circles.

The predictions of the model match well the results from the simulations. We note that since the size of region 2 was chosen to be $2.5 \times 2.5 \times 2.5\ a_0^{\text{Fe}}$, the model should not be used to predict the behavior of smaller box sizes. Additionally, the model was developed under the assumption that there is no interaction between the Ti atoms, which might not be the case for very high Ti concentrations.

Figure 3 shows a histogram of the projected positions, on the **xy** plane, of the C atom during one of the simulations performed in a periodic box of size $5 \times 5 \times 5\ a_0^{\text{Fe}}$ at a temperature of 1023.15 K. The more opaque, the longer the time the C atom has spent in a given location. The substitutional Ti atom is located in the center of the simulation box, while the Fe atoms are omitted for clarity.

Consistent with the calculated negative value of the binding energy in region 2 (E_2), the C atom tends to spend more time inside that region than in the surrounding bulk. Additionally, we note that the C atom does not seem to often visit the octahedral sites adjacent to the Ti atom, which can be explained by the slightly higher value measured for the migration barrier ε_2. Such behavior is a consequence of the Ti-C first-neighbor repulsion which arises due to lattice distortions caused by Ti. Since the misfit volume caused by the presence of Ti is positive (expansion, $\Delta V = 2.19\ \text{Å}^3$), the atomic distances adjacent to Ti will be smaller—the surrounding Fe lattice constrains the full relaxation. Our description is confirmed by a close examination of the simulated lattice spacing around Ti.

Measurements of the separation between atoms along the $\langle 100 \rangle$ directions at 0 K yield indeed that, in the close vicinity of the Ti atom, the interatomic distances are modified. The distance to the second-nearest-neighbor is reduced from $a_0^{\text{Fe}} = 2.864\ \text{Å}$ [29] to 2.823 Å. And the distance to the next atoms in the same directions increases to 2.906 Å.

A shorter distance between the Ti atom and its second-nearest neighbors explains why the C atom is rarely found in its vicinity: there is less space available. Similarly, the greater distance between the second-nearest neighbors of the Ti atom and the subsequent atoms along the $\langle 100 \rangle$ directions explains why the C atom is more often found in such positions.
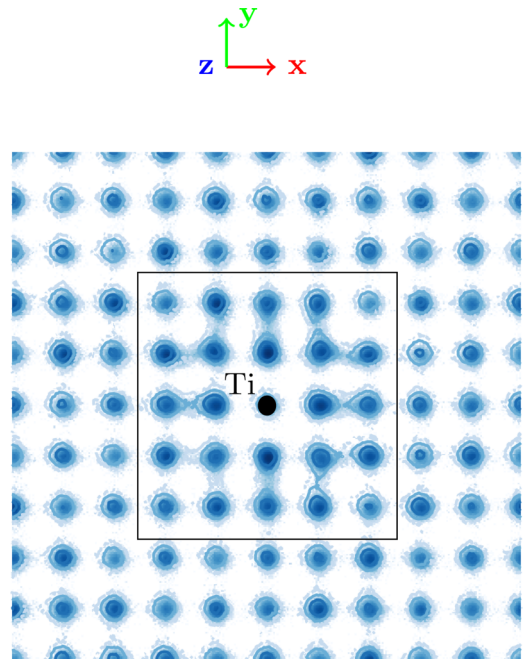

FIG. 3. Logarithmic histogram of the projected positions of the C atom on the **xy** plane during an MD simulation in a system containing a Ti substitutional atom. The opacity of the blue regions is related to the time that the C atom was in a given position. The black square centered in the Ti atom outlines region 2.
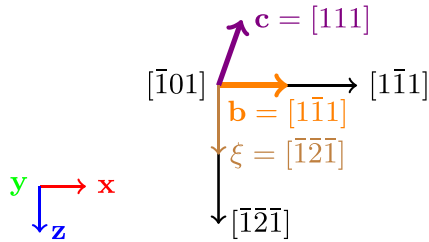
FIG. 4. Orientation of one of the edge dislocations of the dipole inside the simulation box. ξ is the dislocation line, **b** is the Burgers vector, and **c** the conjugate direction.

In the last test case, we evaluate the robustness of the model to predict C diffusion as a function of dislocation density. Once again, we divide the system in two regions: region 2 containing the dislocation line, and region 1, surrounding region 2, containing the remaining atoms. We adopt the Cartesian coordinate system, with the dislocation line along the **z** axis and Burgers vector along the **x** axis (see Fig. 4). We define region 2 to be a square cuboid having the size of the activation distance along **x** and **y**, and the size of the simulation box along **z**. The activation distance has been previously calculated in the literature to be $0.2b - 0.3b$ [4], where b is Burgers vector. We use a value of $0.3b$.

We make the approximation that region 1 can be represented by a bulk structure, and use the energy barrier for migration of C calculated previously; therefore, $\varepsilon_1 = \varepsilon^{\mathrm{EAM}} = 0.79$ eV. For the binding energies, we again use $E_1 = 0$ as a reference.

To calculate the equivalent energy barrier (ε_2) and binding energy (E_2) of region 2, we use a different set of data obtained from MD simulations. We generate systems containing a dipole of edge dislocations using the software available in Ref. [36]; see Fig. 4. The box size used for the simulations at 723 K is $84.56 \times 48.74 \times 7.04$ Å along **x**, **y**, and **z**, respectively, corresponding to a dislocation density of 4.8×10^{16} m^{-2}. Results of diffusivity calculations on these systems, together with a fit to Eq. (4), are presented in Fig. 2(a), marked with the label "Dislocation."

From the fit, we extract an equivalent energy barrier $(\varepsilon_2) = 0.63$ eV and binding energy $(E_2) = -0.60$ eV of region 2. The value of the energy barrier is lower than that in the bulk, indicating that it is easier for a C atom to migrate when it is located in region 2—close or within the dislocation core. The binding energy is negative, which means that the dislocation acts as a trap for the C atom.

We proceed to test its predictive capabilities in terms of changes of the dislocation density and temperature. We construct a set of systems of different sizes containing a dislocation dipole. Since the dislocation line direction (**z**) is periodic, we only modify the other two dimensions. Changing the size of the system while maintaining a single dipole is equivalent to varying the dislocation density—we use $3.7 \times 10^{15}, 9.0 \times 10^{15}, 1.8 \times 10^{16}$, and 4.8×10^{16} m^{-2}. Results of the MD simulations at various temperatures together with the predictions of the model are presented in Fig. 2(c). The data points used for fitting are shown surrounded by circles. The model is able to accurately describe the behavior of C
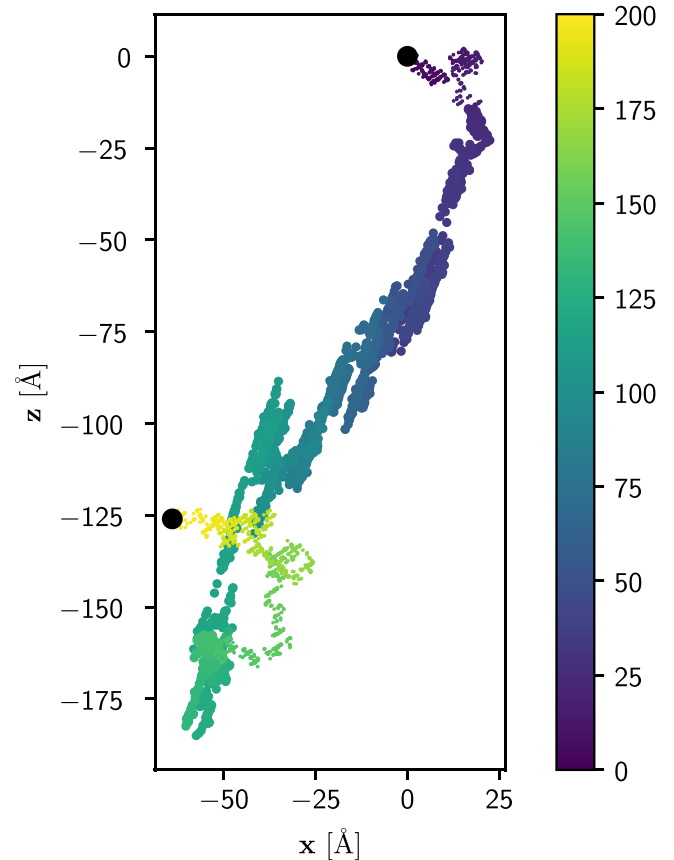

FIG. 5. Position of the C atom projected on the **xz** plane during a simulation in a system containing a dislocation dipole. Larger dots indicate (approximately) when that carbon atom is jointly diffusing with the dislocation. The color bar indicates the simulation time, the units being [ns].

on systems containing dislocations at different dislocations densities and temperatures.

In Fig. 5, we show the diffusive trajectory of the C atom projected on the **xz** plane, the glide plane of the dislocation, for one of the simulations run at 923 K. Even though the periodic simulation box has a size of 7.04 Å along **z**, we show the unwrapped coordinates to have a better insight into the trajectory of the C atom.

The simulation starts with the C atom at the coordinate $(x, z) = (0, 0)$. Initially, the C atom is located in the bulk of the material, where it diffuses between octahedral sites for the first $\approx$20 ns. It is then attracted by one of the dislocations of the dipole and remains near its core for about 120 ns. During the final 60 ns of the simulation, the C atom diffuses again freely in the bulk.

During the time the C atom is near the core of the dislocation, it does not remain static; neither does it diffuse along the dislocation line. It diffuses together with the dislocation, in a combined motion, along the well-defined [111] direction (see larger dots in Fig. 5), the so-called conjugate direction. We confirm the conjugate channelling effect first presented in Ref. [12], where the migration of interstitials is accelerated in a conjugate diffusion direction and not along the dislocation

line. A video showing the diffusion of a C atom along with a dislocation can be found in the Supplemental Material.

We have presented an approach for the calculation of interstitial diffusivity in Fe in the presence of point and line defects. The scheme couples classical molecular dynamics to a simple analytical theory. By validating the theory against our computer experiments, we are able to claim that after fitting a few disposable parameters, analytical results are immediately obtained for diffusion in the presence of any number of defects in any concentration.

We have demonstrated our method for the case of C diffusion in Fe in the presence of dissolved titanium and the presence of different densities of edge dislocations. We find that C is trapped in the vicinity of the Ti atom as a result of small changes in equilibrium bond length caused by the point defect. In this way, C diffusivity is predicted to be *attenuated* by dissolved Ti.

Diffusion of C near an edge dislocation leads to a cooperative migration of both defects. The result is that a conjugate migration direction is introduced which depends on the line sense of the dislocation, see Fig. 4. At the heart of this phenomenon is the reduction in kink formation energy mediated by C binding near the dislocation core.

We expect this method to have wide-ranging applications in the future, in cases of diffusion of C, hydrogen, nitrogen, and boron in multicomponent alloys with nontrivial dislocation microstructures.

[1] World Steel Association, https://worldsteel.org/about-steel/steel-facts?fact=36, accessed on 20-09-2022.

[2] World Steel Association, https://worldsteel.org/steel-stories/innovation/spacex-relies-on-stainless-steel-for-starship-mars-rocket/, accessed on Sept. 20, 2022.

[3] K. Tapasa, A. Barashev, D. Bacon, and Y. Osetsky, Acta Mater. **55**, 1 (2007).

[4] K. Tapasa, Y. Osetsky, and D. Bacon, Acta Mater. **55**, 93 (2007).

[5] R. Veiga, M. Perez, C. Becquart, E. Clouet, and C. Domain, Acta Mater. **59**, 6963 (2011).

[6] R. G. A. Veiga, M. Perez, C. S. Becquart, C. Domain, and S. Garruchet, Phys. Rev. B **82**, 054103 (2010).

[7] A. Ishii, S. Ogata, H. Kimizuka, and J. Li, Phys. Rev. B **85**, 064303 (2012).

[8] O. A. Restrepo, N. Mousseau, F. El-Mellouhi, O. Bouhali, M. Trochet, and C. S. Becquart, Comput. Mater. Sci. **112**, 96 (2016).

[9] S. Fukuhara, K. M. Bal, E. C. Neyts, and Y. Shibuta, Comput. Mater. Sci. **177**, 109581 (2020).

[10] D. Simonovic, C. K. Ande, A. I. Duff, F. Syahputra, and M. H. F. Sluiter, Phys. Rev. B **81**, 054116 (2010).

[11] P. Liu, W. Xing, X. Cheng, D. Li, Y. Li, and X.-Q. Chen, Phys. Rev. B **90**, 024103 (2014).

[12] A. Ishii, J. Li, and S. Ogata, PLoS One **8**, e60586 (2013).

[13] S. Echeverri Restrepo, H. Lambert, and A. T. Paxton, Phys. Rev. Mater. **4**, 113601 (2020).

[14] See Supplemental Material at http://link.aps.org/supplemental/10.1103/PhysRevMaterials.6.L100801 for detailed methods for the diffusivity calculations.

[15] G. P. M. Leyson, W. A. Curtin, L. G. Hector, and C. F. Woodward, Nat. Mater. **9**, 750 (2010).

[16] J. Song and W. Curtin, Nat. Mater. **12**, 145 (2013).

[17] Z. Wu and W. Curtin, Nature (London) **526**, 62 (2015).

[18] S. Plimpton, J. Comput. Phys. **117**, 1 (1995).

[19] S. Echeverri Restrepo, M. H. Sluiter, and B. J. Thijsse, Comput. Mater. Sci. **73**, 154 (2013).

[20] M. I. Mendelev and Y. Mishin, Phys. Rev. B **80**, 144111 (2009).

[21] P. Hirel, Comput. Phys. Commun. **197**, 212 (2015).

[22] M. S. Daw and M. I. Baskes, Phys. Rev. B **29**, 6443 (1984).

[23] M. S. Daw and M. I. Baskes, Phys. Rev. Lett. **50**, 1285 (1983).

[24] G. J. Ackland, M. I. Mendelev, D. J. Srolovitz, S. Han, and A. V. Barashev, J. Phys.: Condens. Matter **16**, S2629 (2004).

[25] C. Becquart, J. Raulot, G. Bencteux, C. Domain, M. Perez, S. Garruchet, and H. Nguyen, Comput. Mater. Sci. **40**, 119 (2007).

[26] R. Veiga, C. Becquart, and M. Perez, Comput. Mater. Sci. **82**, 118 (2014).

[27] M. I. Baskes, Phys. Rev. B **46**, 2727 (1992).

[28] B.-J. Lee and M. I. Baskes, Phys. Rev. B **62**, 8564 (2000).

[29] B.-J. Lee, M. Baskes, H. Kim, and Y. Koo Cho, Phys. Rev. B **64**, 184102 (2001).

[30] H.-K. Kim, W.-S. Jung, and B.-J. Lee, Acta Mater. **57**, 3140 (2009).

[31] T. Schneider and E. Stoll, Phys. Rev. B **17**, 1302 (1978).

[32] B. Dünweg and W. PAUL, Int. J. Mod. Phys. C **02**, 817 (1991).

[33] B.-J. Lee, Acta Mater. **54**, 701 (2006).

[34] W. Pascheto and G. P. Johari, Metall. Mater. Trans. A **27**, 2461 (1996).

[35] Y. Osetsky, Defect Diffus. Forum **188-190**, 71 (2001).

[36] https://github.com/sebastianecheverrir/DipolesMixedDislocations.